CHAPTER 3

EFFECT OF NONLINEAR RADIATION ON MHD FLUID FLOW CONSIDERING MASS TRANSFER

Content of this chapter is published in:

International Journal of Ambient Energy (Taylor and Fransis)
2022, Volume 43(1) 6909-6918 **(Scopus)**

Chapter 3

Effect of nonlinear radiation on MHD fluid flow considering mass transfer

Mass transfer phenomena is found everywhere in nature. The transport of one component in a mixture from a region of higher concentration to one of lower concentration is called mass transfer. Mass transfer finds application in industrial and chemical engineering processes. Such a flow caused by density difference which in turn caused by concentration difference is known as mass transfer flow. Some examples of mass transfer flow are evaporation of water from pond, lake, water reservoir to the atmosphere, separation of chemical species in distillation columns, the diffusion of impurities in rivers, oceans, etc. Radiation plays a significant part in operations involving high temperatures, such as polymer processing, nuclear power plants, glass making, gas turbines, etc.

3.1 Introduction of the Problem

Mass transfer refers to the net movement of material due to species concentration gradient. The process of mass transfer is broadly applicable in populous areas of science, engineering and technology. The performance of mass transfer is widely associable in electrical engineering, environmental engineering, metallurgy, air conditioning and biological functions. In biological operations namely respiratory mechanisms, blood distillation, osmosis as well as metabolism of blood and drugs. It can be found in ablative coding, cooling of rocket and jet mechanisms. Natural convection flow of MHD fluid with mass transfer over stretching sheet have been scrutinized by Afify [2]. Nayak et al. [82] investigated mass transfer effect on MHD fluid over a stretching sheet.

At high temperatures, radiative heat transmission becomes increasingly important. It has a wide range of uses, including nuclear power plants, gas turbines, propulsion systems for spacecraft, missiles, and aeroplanes, as well as breakthroughs in hypersonic flight and gas-cooled nuclear devices for interplanetary flight. Farooq et al. [69] examined viscoelastic fluid flow with nonlinear radiation and convective boundary conditions. Khan and Alzahrani [74] examines influence of nonlinear thermal radiative on MHD fluid flow. Khan et al. [75] deals with entropy generation in fluid flow over stretchable surface. Nayak et al. [79] found entropy generation effects on MHD flow of fluid subject to convective boundary conditions. Wang et al. [50] scrutinized entropy optimized MHD Viscous liquid flow with heat generation/absorption and Joule heating effects. Yusuf et al. [130] studied the rate of entropy generation of MHD fluid flow over stretching plate. Elkoumy et al. [117] investigated Magnetic Field Effects on MHD Fluid through a Porous Medium. Gowda et al. [107] studied the steady MHD fluid flow with heat and mass transfer characteristics. Wang et al. [34] explored effect of thermal transport phenomena of MHD fluid flow over vertical plate. Sarada et al. [60] proposed a mathematical model to describe the flow, heat and mass transfer behaviour of a non-Newtonian fluid over a stretching sheet.

3.2 Novelty of the Chapter

The main objective of the present work to develop mathematical modelling of heat generation/absorption effects on Entropy optimized MHD fluid flow with mass transfer in the presence of nonlinear radiation. The simplified systems of ordinary differential equations are solve using the Homotopy analysis method.

3.3 Mathematical Formulation of the Problem

Consider steady, two dimensional, incompressible, natural convection MHD flow of electrically conducting fluid with first order velocity slip over vertical stretching sheet as displayed in Figure 3.1. The mathematical model is considered under the following assumptions and conditions.

- Total entropy subject to heat transfer irreversibility, joule heating irreversibility, viscous dissipation irreversibility and mass diffusion irreversibility are calculated via second law of thermodynamics.
- Induced magnetic field is negligible via small Reynolds number.

- Energy equation mathematically modelled subject to viscous dissipation, joule heating effect, heat generation/absorption and nonlinear radiation.
- Convective boundary condition is applied to the boundary.
- A constant magnetic field of strength $\mathcal{B} = B_0$ is applied in the opposite to the direction of the flow.
- Let us suppose that $u = U_w + U_{Slip} = ax + l\dfrac{\partial u}{\partial y}$ is the stretching velocity with initial stretching rate $a > 0$.

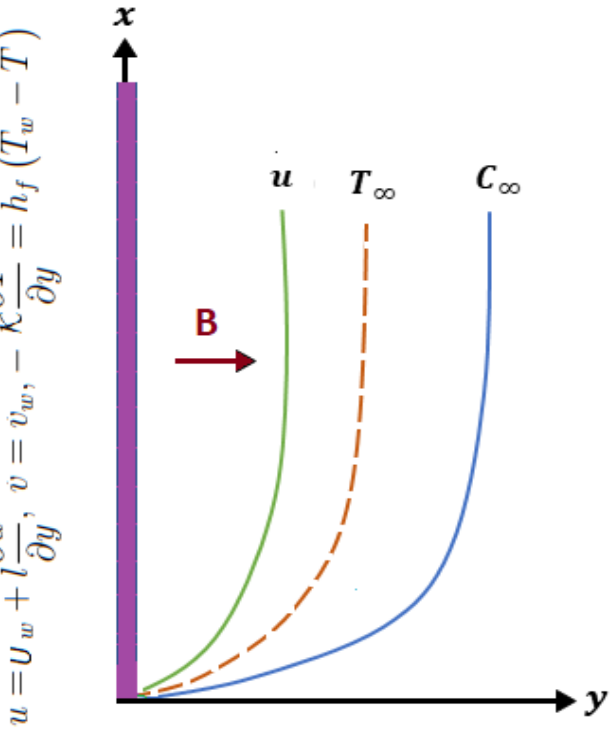

Figure 3.1: Physical sketch

Under the aforementioned assumptions and usual Boussinesq approximations, the governing equations are:

$$\frac{\partial u}{\partial x} + \frac{\partial v}{\partial y} = 0, \tag{3.3.1}$$

$$u\frac{\partial u}{\partial x} + v\frac{\partial u}{\partial y} = \nu\frac{\partial^2 u}{\partial y^2} - \frac{\sigma B_0^2}{\rho}u + g\beta_T(T - T_\infty) + g\beta_C(C - C_\infty), \tag{3.3.2}$$

$$\rho C_p\left(u\frac{\partial T}{\partial x} + v\frac{\partial T}{\partial y}\right) = \kappa\frac{\partial^2 T}{\partial y^2} + \mu\left(\frac{\partial u}{\partial y}\right)^2 + \sigma B_0^2 u^2 + Q^*(T - T_\infty) - \frac{\partial q_r}{\partial y}, \tag{3.3.3}$$

$$u\frac{\partial C}{\partial x}+v\frac{\partial C}{\partial y}=D_M\frac{\partial^2 C}{\partial y^2} \tag{3.3.4}$$

with boundary conditions

$$\left.\begin{array}{l} u=U_w+U_{Slip},\ v=v_w,\ -\kappa\dfrac{\partial T}{\partial y}=h_{ft}\left(T_w-T_\infty\right),\ C=C_w\ \text{ at }\ y=0. \\ u\to 0,\ T\to T_\infty\ C\to C_\infty\ \text{ as }\ y\to\infty. \end{array}\right\} \tag{3.3.5}$$

here first order velocity slip in above boundary condition Eq. 3.3.5 is mathematically expressed as $U_{Slip}=l\dfrac{\partial u}{\partial y}$, where l is free mean molecular path.
Radiative heat flux [126] is:

$$q_r=-\frac{4\sigma^*}{3k^*}\frac{\partial T^4}{\partial y}, \tag{3.3.6}$$

Where σ^* and k^* are the Stefan Stefan-Boltzmann constant and mean absorption coefficient respectively. Now, it can be linearized by considering small temperature differences within the flow such that expanding T^4 with the help of the Taylor series about T_∞ and neglecting higher order terms in the above equation, we get

$$q_r=-\frac{16\sigma^* T_\infty^3}{3k^*}\frac{\partial T}{\partial y}, \tag{3.3.7}$$

The above equation represents to linear thermal radiation, but the intension of the current study is to explore the impact of non-linear thermal radiation, so we replace T_∞^3 with T^3 in Equation (3.3.7)

$$q_r=-\frac{16\sigma^* T^3}{3k^*}\frac{\partial T}{\partial y}, \tag{3.3.8}$$

differentiating equation (3.3.8) with respect to y, we get

$$\frac{\partial q_r}{\partial y}=-\frac{16\sigma^*}{3k^*}\left[3T^2\left(\frac{\partial T}{\partial y}\right)^2+T^3\frac{\partial^2 T}{\partial y^2}\right], \tag{3.3.9}$$

Following similarity transformations are used to covert system of partial differential equations (3.3.1)-(3.3.5), into system of ordinary differential equations

$$\eta=\sqrt{\frac{a}{\nu}}y,\ \psi=\sqrt{a\nu}\ xf\left(\eta\right),\ \ \theta\left(\eta\right)=\frac{T-T_\infty}{T_w-T_\infty},\quad \phi\left(\eta\right)=\frac{C-C_\infty}{C_w-C_\infty}, \tag{3.3.10}$$

where ψ is the stream function, so we get velocity components given as

$$u=\frac{\partial\psi}{\partial y}=axf'\left(\eta\right),\ v=-\frac{\partial\psi}{\partial x}=-\sqrt{a\nu}\ f\left(\eta\right), \tag{3.3.11}$$

Now using Equations (3.3.9)-(3.3.11), for converting system of partial differential Equations (3.3.1)-(3.3.5) into system of ordinary differential equations, we found continuity equation (3.3.1) is identically satisfied, and dimensionless form of velocity, energy and concentration equations are given as follows:

$$f''' + ff'' - (f')^2 - Mf' + Gr_T\theta + Gr_C\phi = 0, \tag{3.3.12}$$

$$\left[1 + \frac{4}{3}Rd\left\{1 + (\theta_w - 1)\,\theta\right\}^3\right]\theta'' + 4Rd\left\{1 + (\theta_w - 1)\,\theta\right\}^2(\theta_w - 1)\,\theta'^2 + Prf\theta' + Brf''f'' + MBrf'f' + Pr\beta\theta = 0, \tag{3.3.13}$$

$$\phi'' + Scf\phi' = 0, \tag{3.3.14}$$

with

$$f(0) = f_w, \quad f'(0) = 1 + \gamma f''(0), \quad \theta'(0) = -\lambda_1(1 - \theta(0)), \quad \phi(0) = 1 \ \text{ at } \ \eta = 0,$$
$$f'(\eta) \to 0, \ \theta(\eta) \to 0, \ \phi(\eta) \to 0 \ \text{ as } \ \eta \to \infty, \tag{3.3.15}$$

where $Gr_T = \dfrac{g\beta_T(T_w - T_\infty)}{a^2x}$, $Gr_C = \dfrac{g\beta_C(C_w - C_\infty)}{a^2x}$, $M = \dfrac{\sigma B_0^2}{a\rho}$, $Pr = \dfrac{\mu C_p}{\kappa}$, $Rd = \dfrac{4\sigma^* T_\infty^3}{3k^*\kappa}$, $f_w = -\dfrac{v_w}{\sqrt{a\nu}}$, $\gamma = l\sqrt{\dfrac{a}{\nu}}$, $Ec = \dfrac{U_w^2}{C_p(T_w - T_\infty)}$, $\beta = \dfrac{Q^*}{a\rho C_p}$, $\lambda_1 = \sqrt{\dfrac{\nu}{a}}\dfrac{h_{ft}}{\kappa}$, $Sc = \dfrac{\nu}{D_M}$, $\theta_w = \dfrac{T_w}{T_\infty}$, $Br = PrEc$.

The dimensional form of Skin friction coefficient, Nusselt number and Sherwood number are

$$C_{fx} = \frac{\tau_w}{\rho U_w^2}\ , \ Nu_x = \frac{xq_w}{\kappa\,(T_w - T_\infty)} \ \text{ and } \ Sh_x = \frac{xq_m}{D_M\,(C_w - C_\infty)}, \tag{3.3.16}$$

where shear stress $\tau_w = \mu\left(\dfrac{\partial u}{\partial y}\right)_{y=0}$, heat flux $q_w = -\kappa\left(1 + \dfrac{16\sigma^* T^3}{3k^*\kappa}\right)\left(\dfrac{\partial T}{\partial y}\right)_{y=0}$ and mass flux $q_m = -D_M\left(\dfrac{\partial C}{\partial y}\right)_{y=0}$. So, dimensionless form of physical interest becomes

$$C_{fx}Re_x^{\frac{1}{2}} = f''(0)\,, Sh_xRe_x^{-\frac{1}{2}} = -\phi'(0)\,, \tag{3.3.17}$$

$$Nu_xRe_x^{-\frac{1}{2}} = -\left(1 + \frac{4}{3}Rd\left\{1 + (\theta_w - 1)\,\theta(0)\right\}^3\right)\theta'(0), \tag{3.3.18}$$

in which $Re_x = \dfrac{x\,U_w}{\nu}$ shows Reynolds number.

Dimensional form of entropy generation is

$$S_G = \frac{\kappa}{T_\infty^2}\left(1+\frac{16\sigma^* T^3}{3\kappa k^*}\right)\left(\frac{\partial T}{\partial y}\right)^2 + \frac{\mu}{T_\infty}\left(\frac{\partial u}{\partial y}\right)^2 + \frac{\sigma B_0^2}{T_\infty}u^2 + \frac{RD}{C_\infty}\left(\frac{\partial C}{\partial y}\right)^2, \quad (3.3.19)$$

now, using Equations (3.3.10)-(3.3.11), the dimensionless form is

$$N_G = \alpha_1\left(1+\frac{4}{3}Rd\left\{1+(\theta_w-1)\,\theta\right\}^3\right)\theta'^2 + Brf''^2 + MBrf'^2 + \left(\frac{L^*}{\alpha_1}\right)\alpha_2\phi'^2, \quad (3.3.20)$$

where R is the ideal gas constant, $L^* = \dfrac{RDC_\infty}{\kappa}$ is diffusion parameter, $\alpha_2 = \left(\dfrac{C_w - C_\infty}{C_\infty}\right)^2$ is concentration ratio parameter.

$$Be = \frac{\text{Heat and mass transfer irreversibilities}}{\text{Total entropty genearation}} \quad (3.3.21)$$

So mathematical expression of Be is given as

$$Be = \frac{\alpha_1\left(1+\frac{4}{3}Rd\left\{1+(\theta_w-1)\,\theta\right\}^3\right)\theta'^2 + \left(\frac{L^*}{\alpha_1}\right)\alpha_2\phi'^2}{\alpha_1\left(1+\frac{4}{3}Rd\left\{1+(\theta_w-1)\,\theta\right\}^3\right)\theta'^2 + Brf''^2 + MBrf'^2 + \left(\frac{L^*}{\alpha_1}\right)\alpha_2\phi'^2} \quad (3.3.22)$$

3.4 Solution by Homotopy Analysis Method

Homotopy method is a basic concept of topology. Liao [120] proposed HAM is used in Equations (3.3.12)-(3.3.14) with boundary conditions (3.3.15). Initial guesses $f_0(\eta)$, $\theta_0(\eta)$, $\phi_0(\eta)$ and auxiliary linear operators $\mathcal{L}_f$, $\mathcal{L}_\theta$, $\mathcal{L}_\phi$ for the HAM solution can be chosen as

$$f_0(\eta) = f_w + \frac{1}{1+\gamma}\left(1-e^{-\eta}\right), \theta_0(\eta) = \frac{\lambda_1}{1+\lambda_1}e^{-\eta}, \phi_0(\eta) = e^{-\eta}, \quad (3.4.1)$$

$$\mathcal{L}_f = \frac{\partial^3 f}{\partial\eta^3} - \frac{\partial f}{\partial\eta}, \mathcal{L}_\theta = \frac{\partial^2\theta}{\partial\eta^2} + \frac{\partial\theta}{\partial\eta}, \mathcal{L}_\phi = \frac{\partial^2\phi}{\partial\eta^2} + \frac{\partial\phi}{\partial\eta} \quad (3.4.2)$$

with $\mathcal{L}_f\left(k_1+k_2e^{\eta}+k_3e^{-\eta}\right)=0$, $\mathcal{L}_\theta\left(k_4+k_5e^{-\eta}\right)=0$, $L_\phi\left(k_6+k_7e^{-\eta}\right)=0$, where $k_1, k_2, \ldots, k_7$ are arbitrary constants.

3.4.1 Convergence Analysis

The solution of the convergence rate in the HAM method depends strongly on parameter $\hbar$. The $f''(0)$, $\theta'(0)$ and $\phi'(0)$ functions are plotted at the 20^{th}-order of approximations to get the allowable values of $\hbar_f$, $\hbar_\theta$ and $\hbar_\phi$. The values of $\hbar_f$, $\hbar_\theta$ and $\hbar_\phi$ are selected in such a way that curves are parallel to $\hbar$-axis. From Figures 3.2-3.4 we can choose $\hbar_f = -1.51$, $\hbar_\theta = -0.22$ and $\hbar_\phi = -0.88$.

3.5 Result and Discussion

This section focuses on the physics of the problem by displaying fluid characteristics graphically. Mathematica is used to obtain solutions. The influence of various parameters on the fluid flow are represented through Figures 3.5-3.19. The following default parameter values are adopted for calculations in the current study: $M = \lambda_1 = Gr_T = Gr_C = 0.1$, $Rd = 0.7$, $Pr = 7.0$, $\gamma = Br = \theta_w = Sc = f_w = 0.5$. As a result, all graphs and tables, unless otherwise specified, are based on these values.

Impact of Magnetic parameter M on velocity profile $f'(\eta)$ as illustrated in Figure 3.5. Here, velocity decreases clearly against M. Figure 3.6 shows behaviour of slip parameter γ on $f'(\eta)$. Velocity is reduced for a larger estimation of γ. Physically, the deformation is slightly transferred to the fluid, resulting in a reduction in the velocity profile. Figure 3.7 represents the influence of suction/injection parameter f_w on $f'(\eta)$. Suction is a substance that improves fluid flow resistance and declines fluid velocity.

Figure 3.8 reveals the positive consequences of Rd on $\theta(\eta)$. Enhancement in Rd releases heat energy in the flow thus enhancing fluid temperature. Figure 3.9 shows the influence of temperature ratio parameter θ_w on $\theta(\eta)$. It is evident from figure that increasing θ_w results in advanced wall temperature to that of ambient temperature. As a result of this, the fluid temperature rises. Figure 3.10 illustrates the influence of Brinkman number Br on $\theta(\eta)$. Br corresponds to slow thermal conductivity produced by viscous dissipation, and as a result, $\theta(\eta)$ rises. Figure 3.11 displays the effect of Prandtl number Pr on $\theta(\eta)$. Since Pr is the ratio of momentum diffusivity to thermal diffusivity, as Pr is increased, thermal diffusivity decreases, resulting in a decrease in $\theta(\eta)$.

Figure 3.12 exhibits significance of Schmidt number Sc on $\phi(\eta)$. It is seen that rise in Sc decreases the fluid concentration. Physically the molecular diffusion decreases with increasing Sc values. The impact of Suction parameter f_w on $\phi(\eta)$ is shown in Figure 3.13. We can see that concentration decreases for the large values

of f_w. Characteristics of Diffusion parameter L^* on N_G and Be is given in Figures 3.14-3.15. Both N_G and Be are enhanced. Influence of Magnetic parameter M on N_G and Be is plotted in Figures 3.16-3.17. N_G is enhanced while Be is decreased against larger values of M. Figures 3.18-3.19 relate N_G and Be with Brinkman number Br. N_G is enhanced while Be is decreased against larger values of Br.

Influence of various parameters M, γ, Gr_T, Gr_C, f_w, Sc, Rd, Pr, Br, θ_w, λ_1 on skin friction, Nusselt and Sherwood numbers are illustrated in Table 3.1, Table 3.2 and Table 3.3. Table 3.1 illustrates that, for rising values of γ and Gr_T, Skin friction factor enhanced while opposite behavior found for large values of f_w, M. Table 3.2 shows that Nusselt number increased for larger approximation of Pr, θ_w and Rd while behaves opposite for large values of Br, M. Table 3.3 illustrates that Sherwood number enhanced for larger approximation of f_w, Sc and behaved opposite for γ.

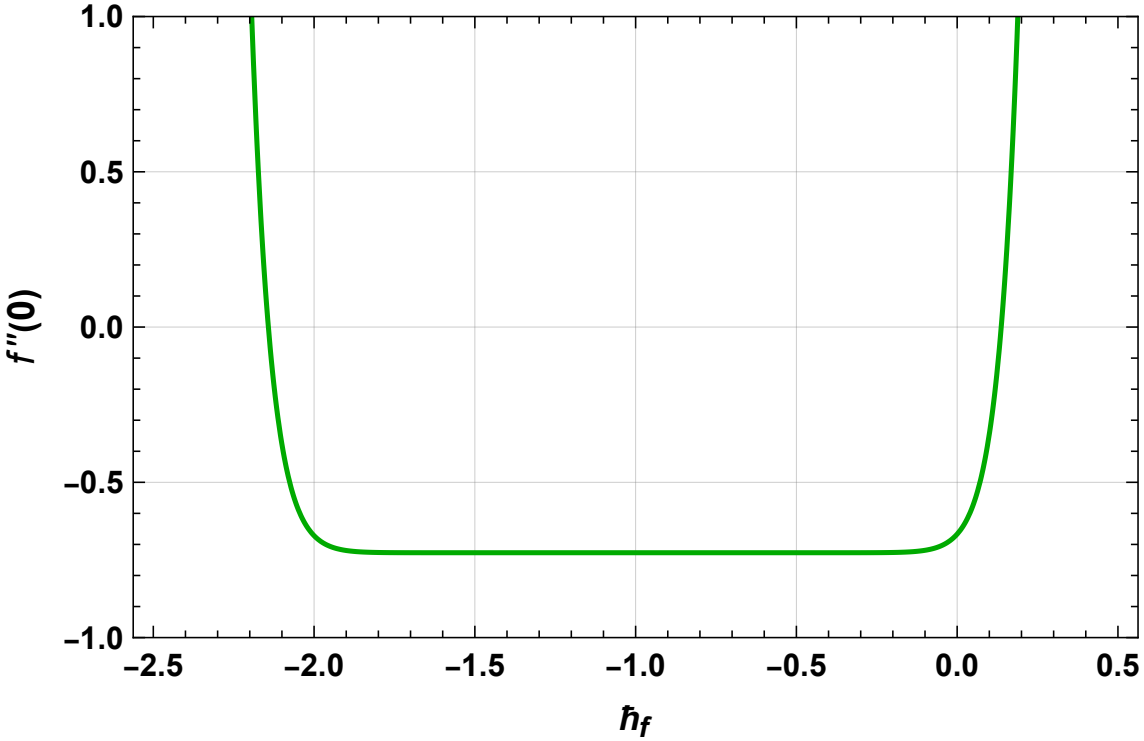

Figure 3.2: $\hbar$-curve for $f''(0)$

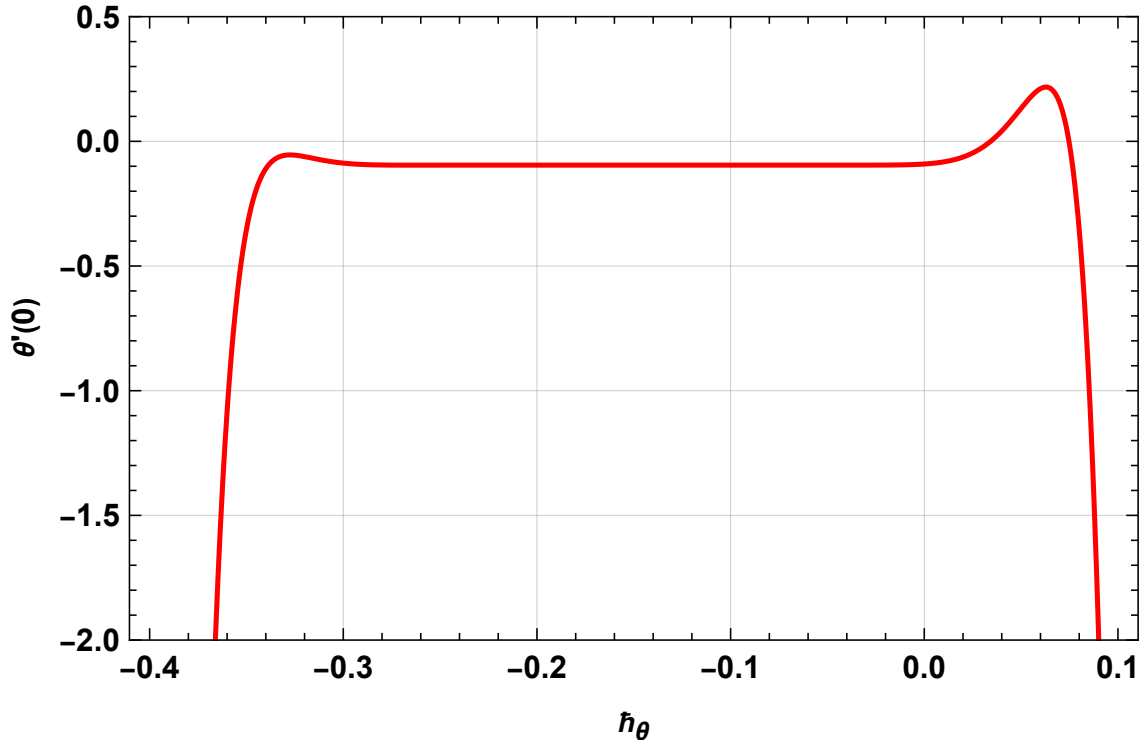

Figure 3.3: $\hbar$-curve for $\theta'(0)$

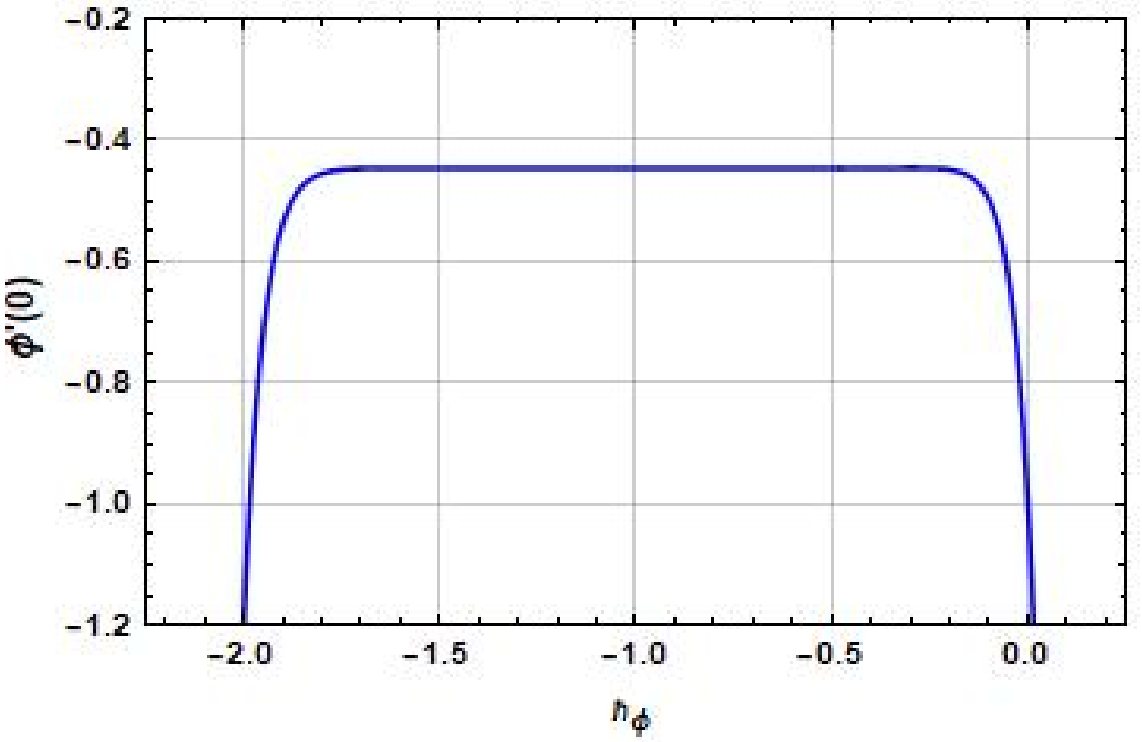

Figure 3.4: $\hbar$-curve for $\theta'(0)$

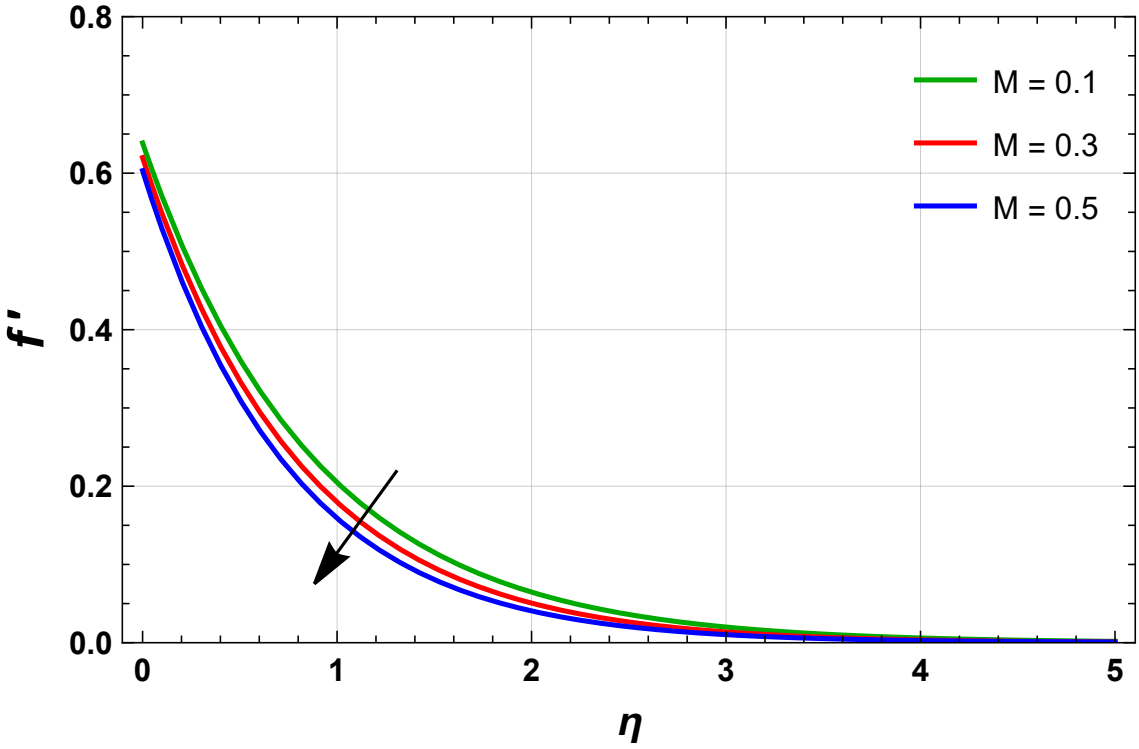

Figure 3.5: $f'(\eta)$ via M

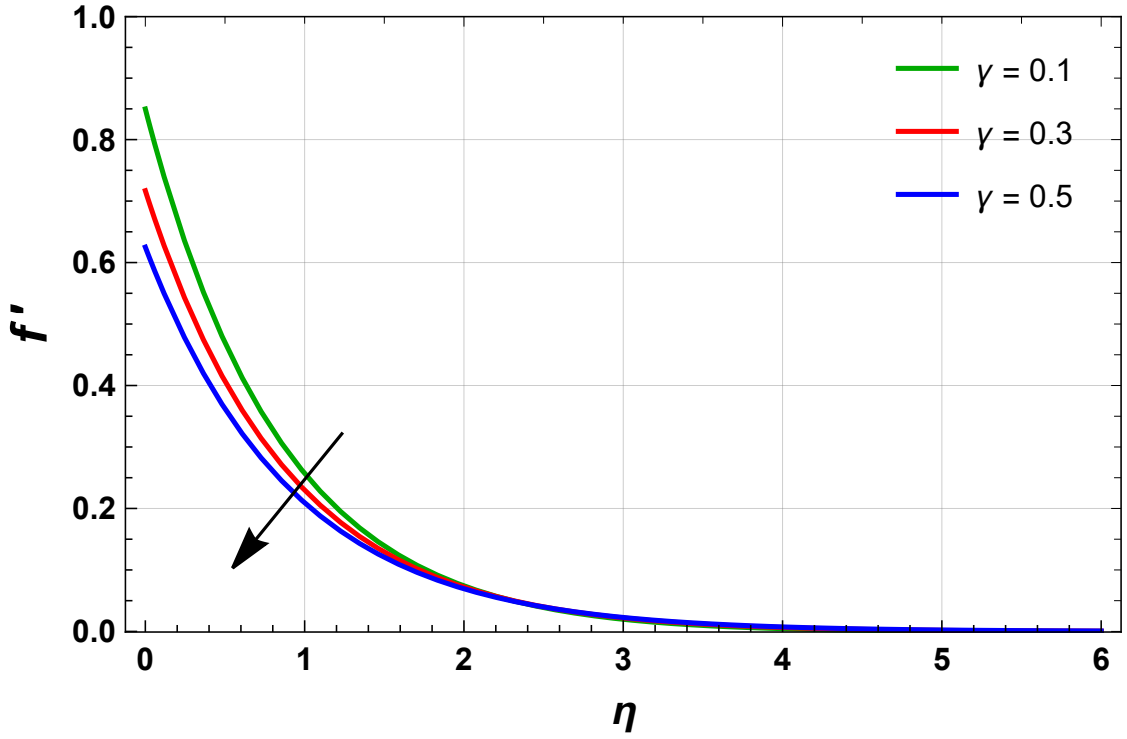

Figure 3.6: $f'(\eta)$ via γ

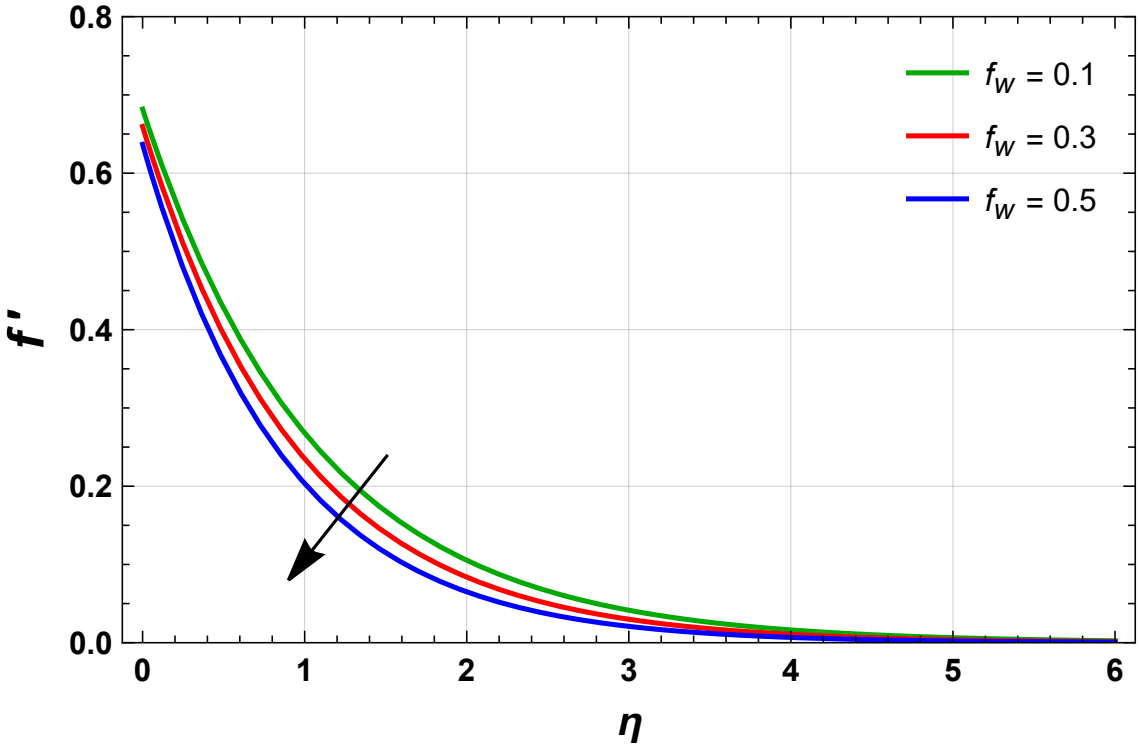

Figure 3.7: $f'(\eta)$ via f_w

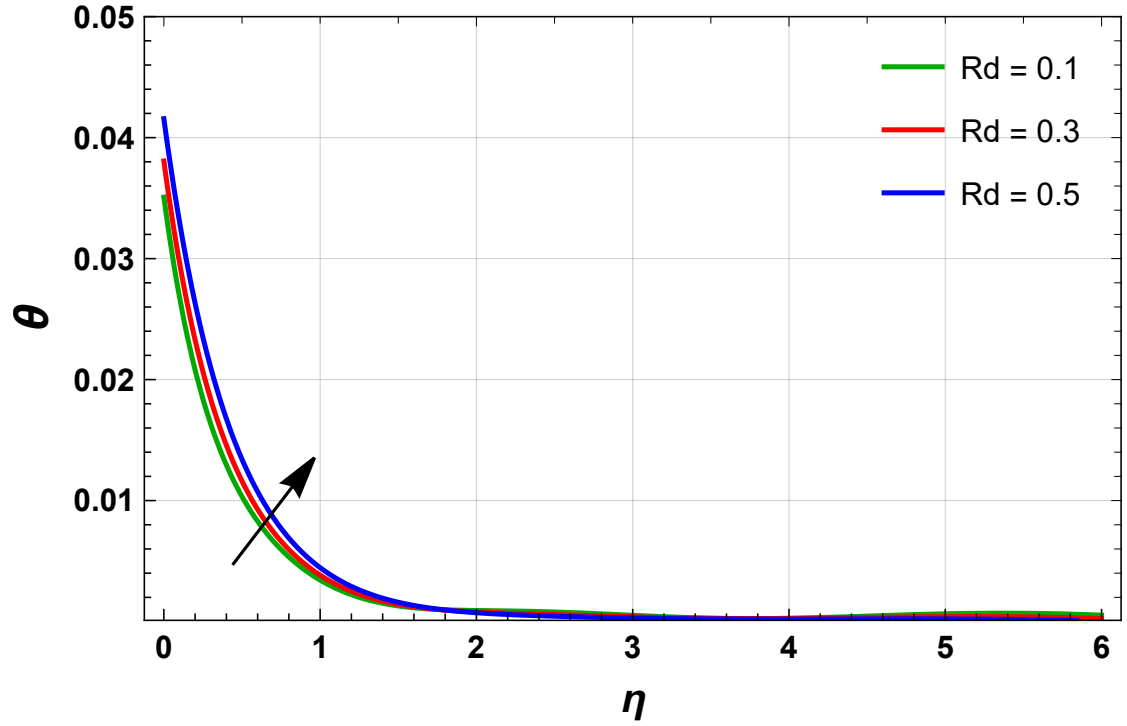

Figure 3.8: $\theta(\eta)$ via Rd

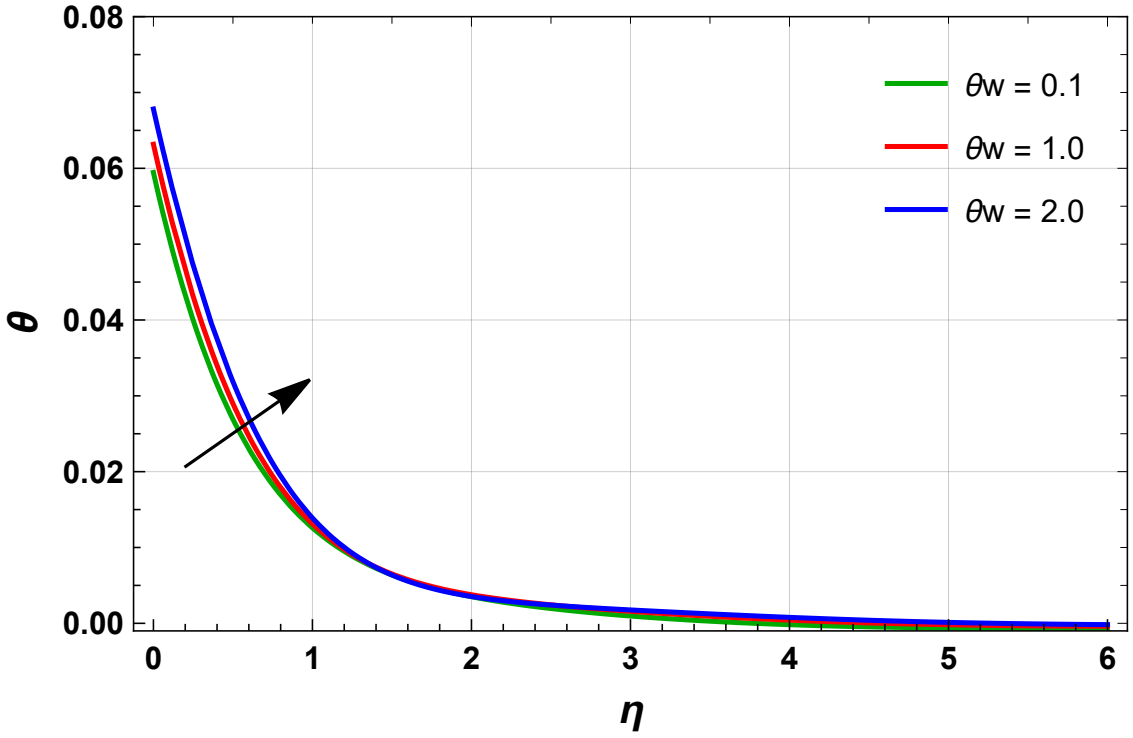

Figure 3.9: $\theta(\eta)$ via θ_w

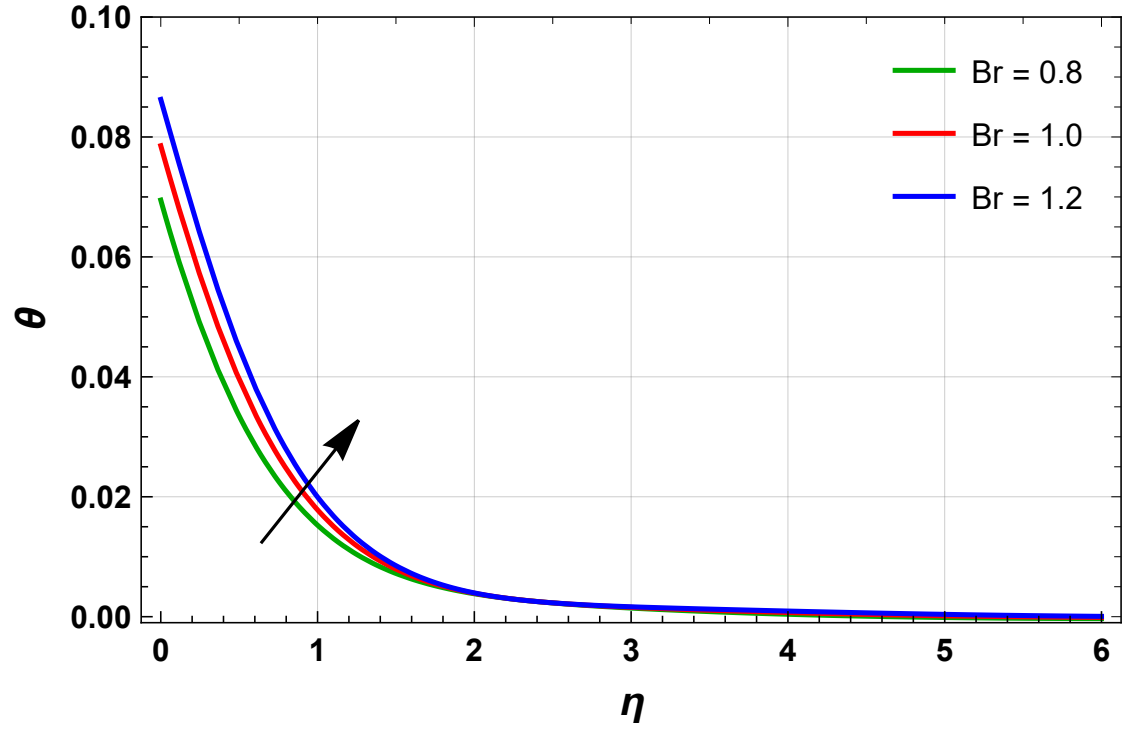

Figure 3.10: $\theta(\eta)$ via Br

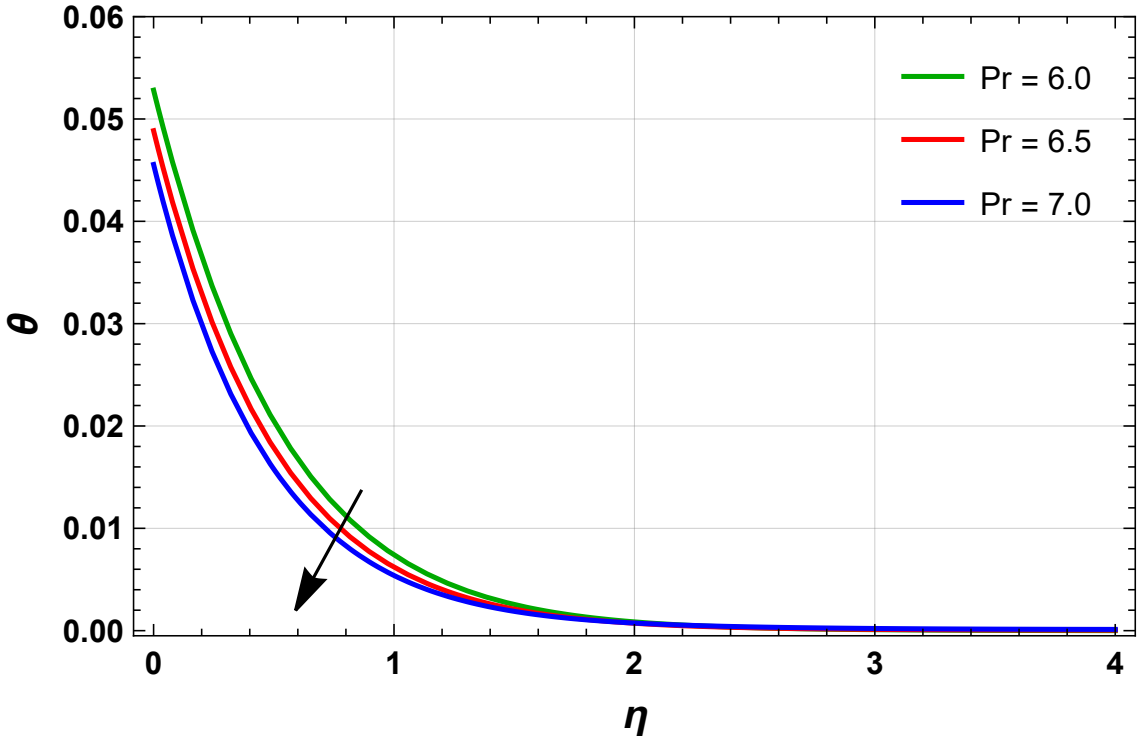

Figure 3.11: $\theta(\eta)$ via Pr

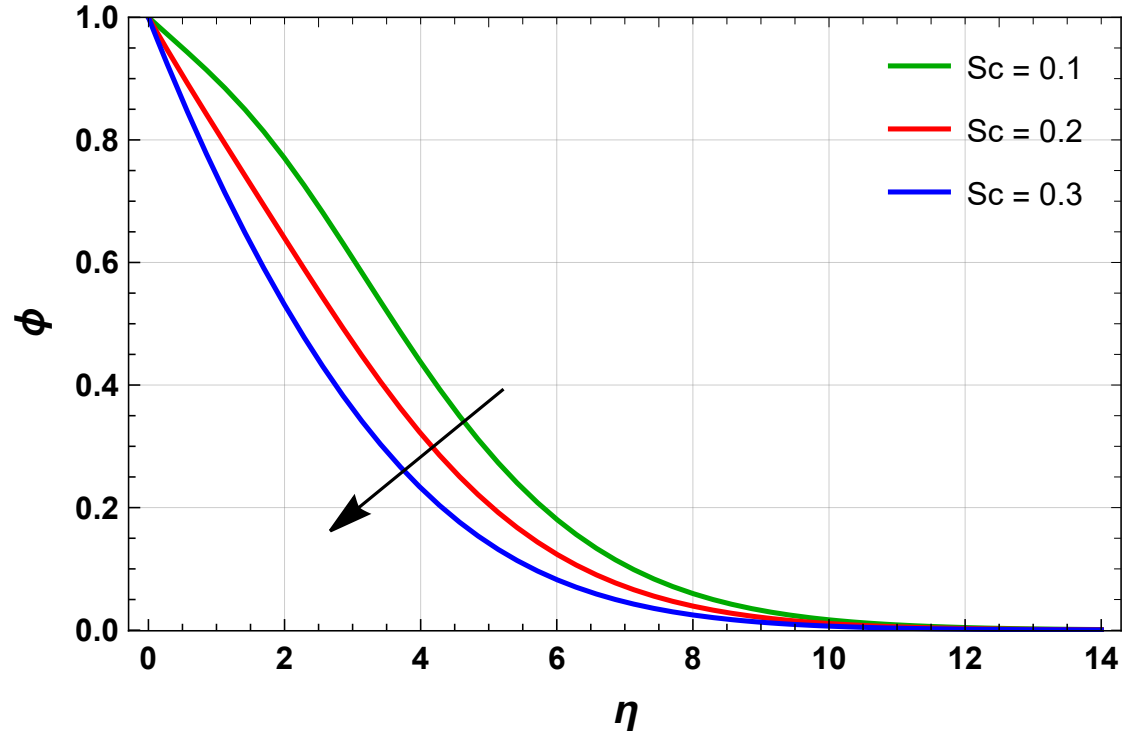

Figure 3.12: ϕ via Sc

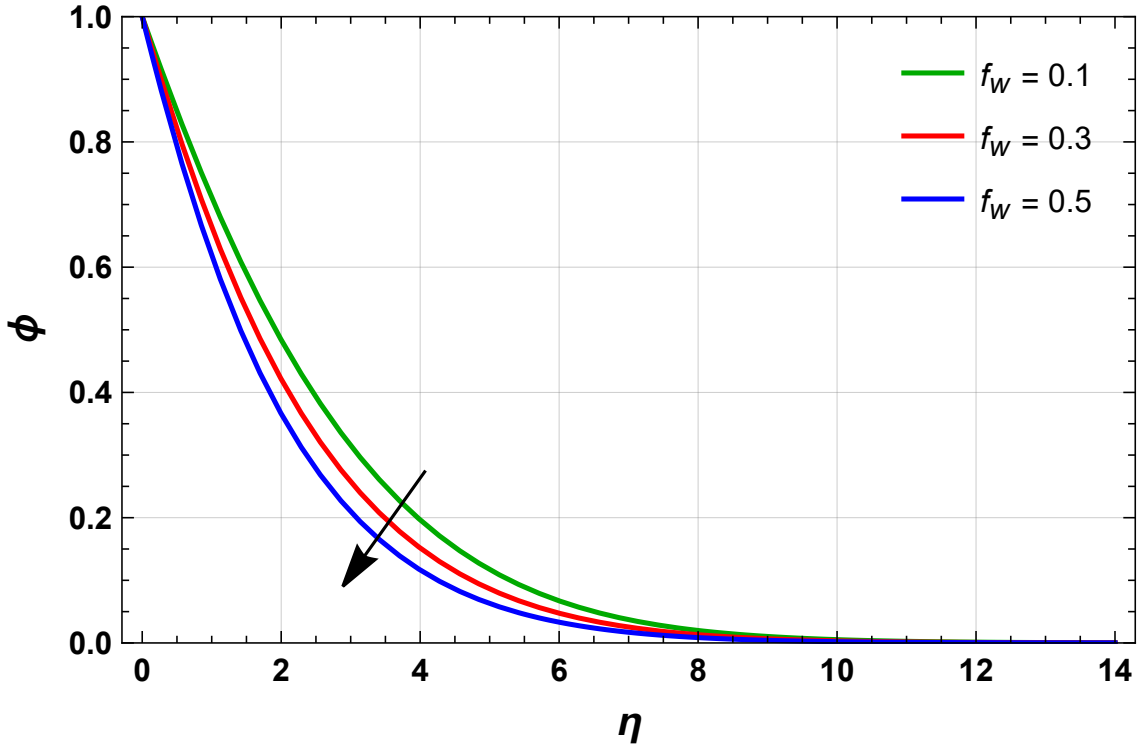

Figure 3.13: ϕ via f_w

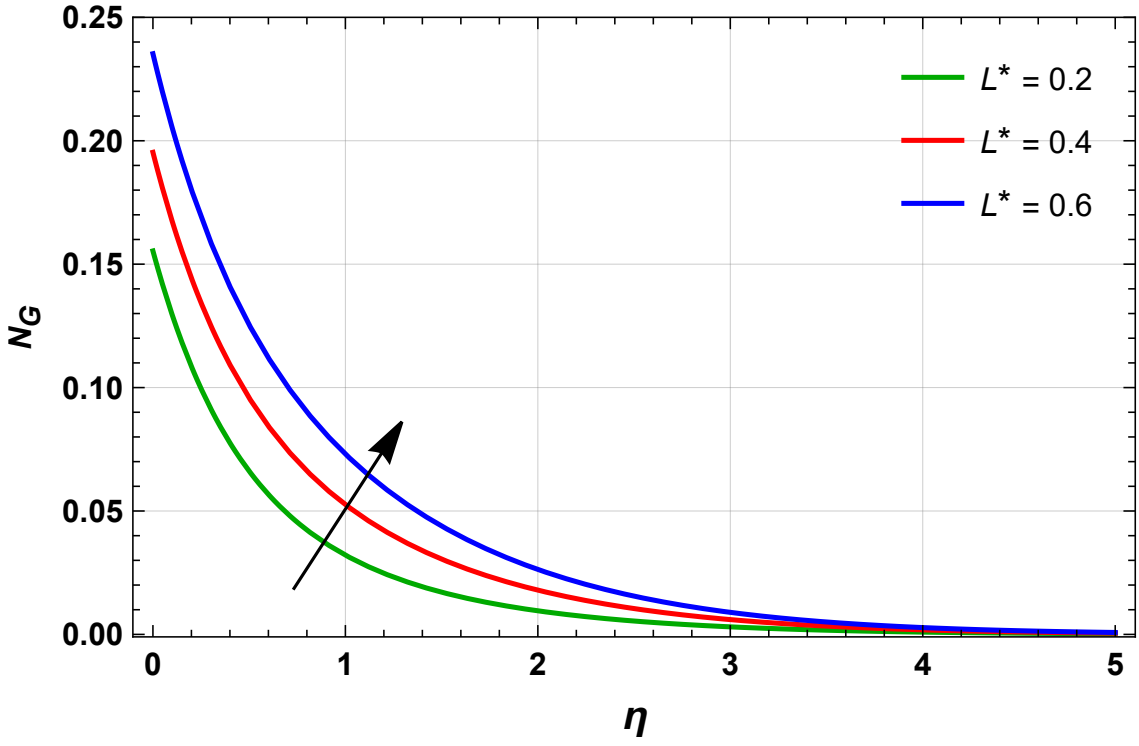

Figure 3.14: N_G via L^*

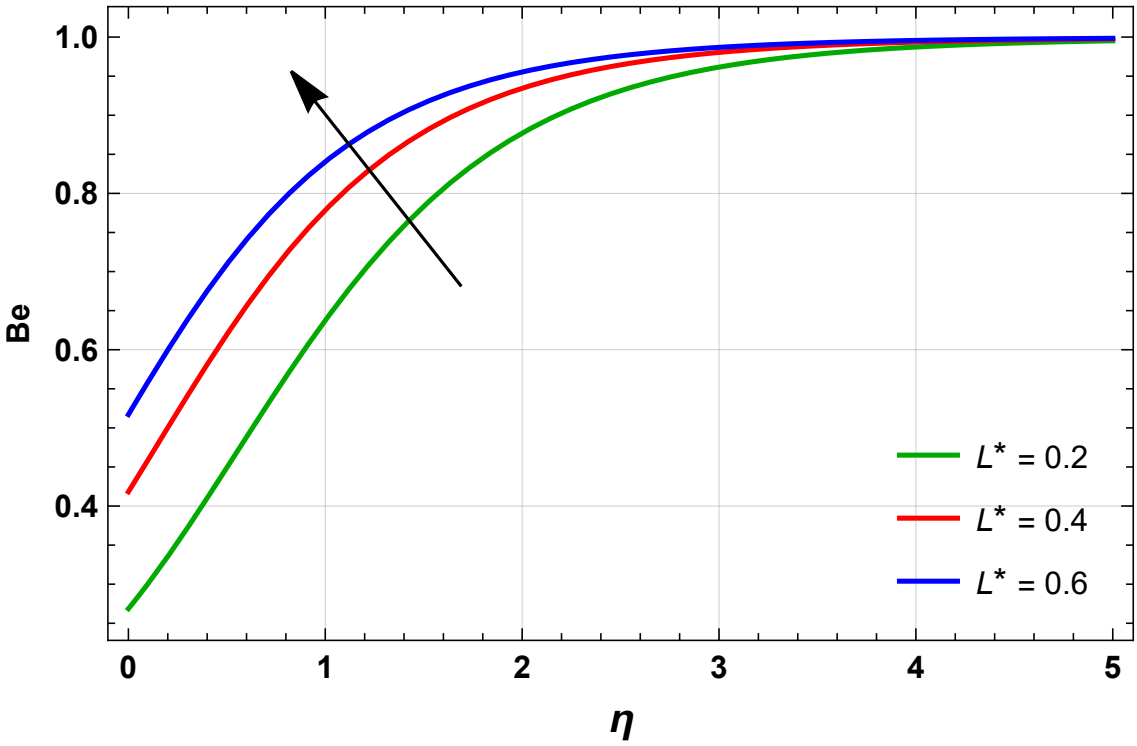

Figure 3.15: Be via L^*

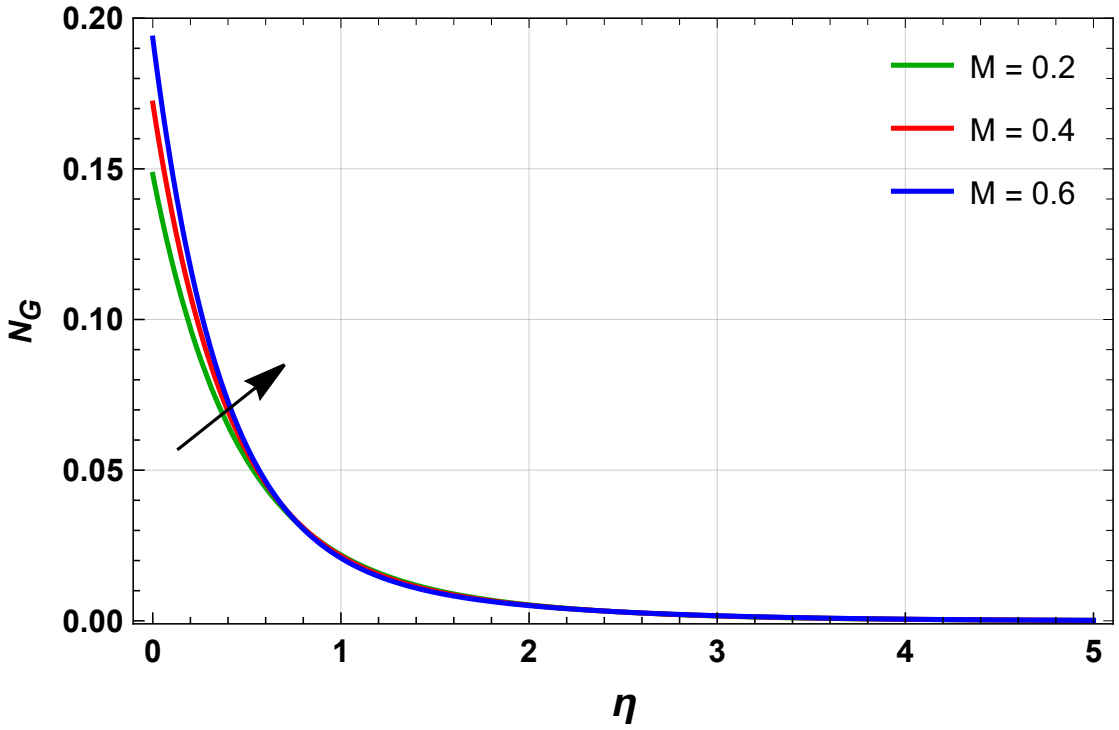

Figure 3.16: N_G via M

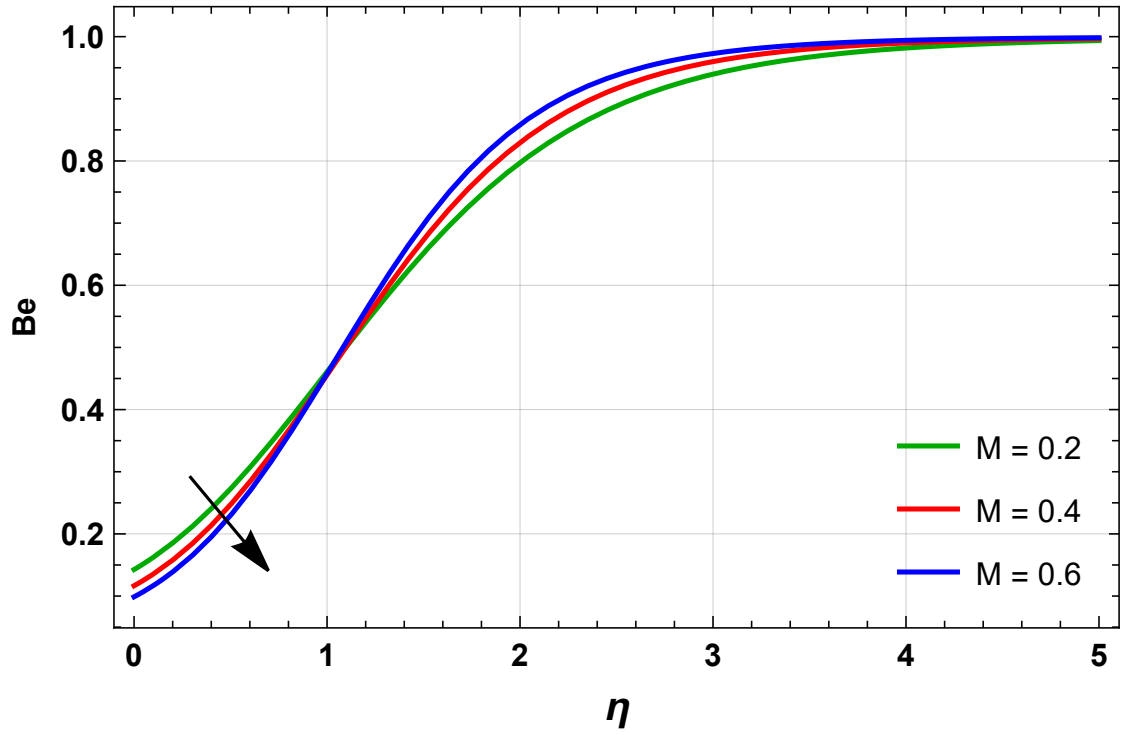

Figure 3.17: Be via M

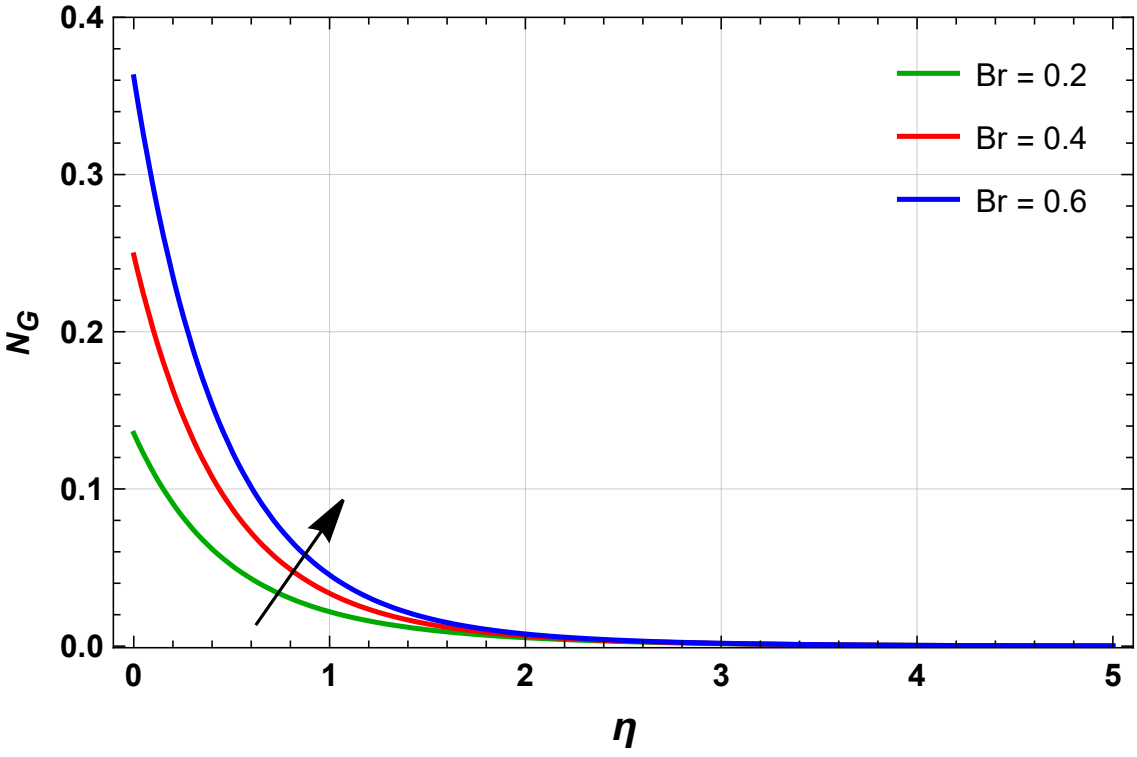

Figure 3.18: N_G via Br

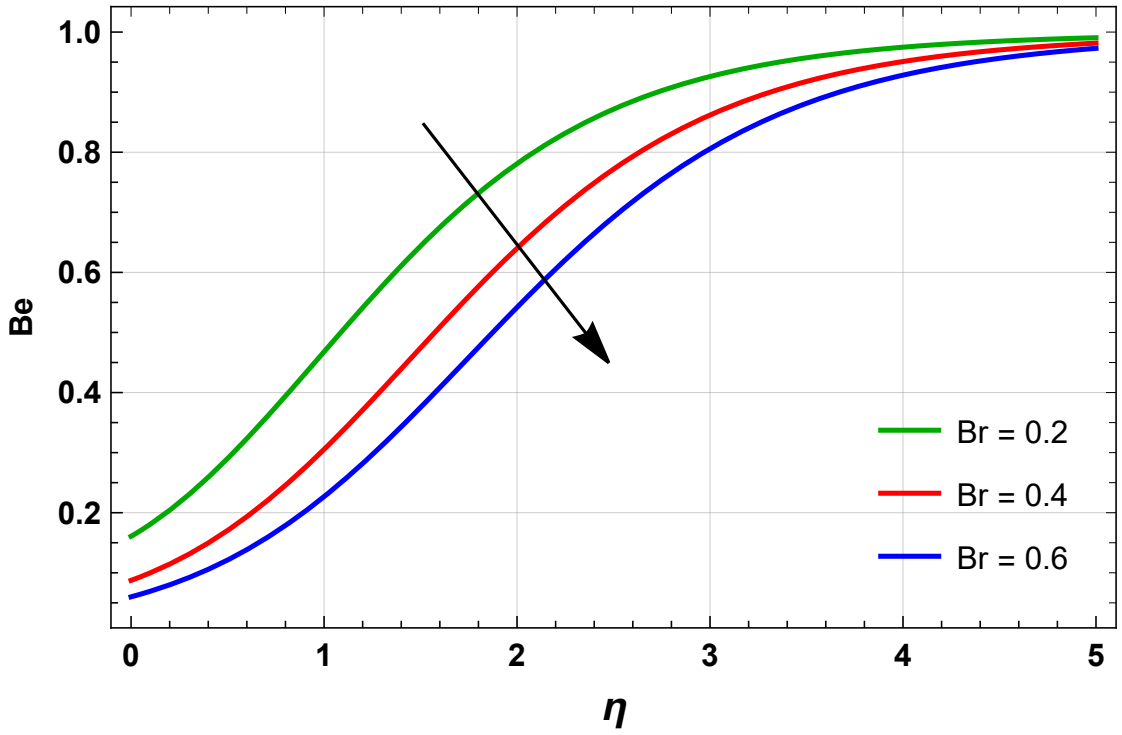

Figure 3.19: Be via Br

Table 3.1: Numerical outcomes of $C_{fx}Re_x^{1/2}$ via various parameters with $\beta = \lambda_1 = Gr_C = 0.1, Br = Sc = \theta_w = 0.5, Pr = 7.0, Rd = 0.7$.

M	γ	Gr_T	f_w	$C_{fx}Re_x^{1/2}$
0.1	0.5	0.1	0.5	-0.68403
0.2				-0.70009
0.3				-0.71772
	0.6			-0.63247
	0.7			-0.58860
		0.2		-0.68173
		0.3		-0.67943
			0.6	-0.70087
			0.7	-0.71772

Table 3.2: Numerical outcomes of $Nu_x Re_x^{-1/2}$ via various parameters with $\beta = \lambda_1 = Gr_T = Gr_C = 0.1, Br = \gamma = Sc = f_w = 0.5$.

M	Rd	θ_w	Br	Pr	$Nu_x Re_x^{-1/2}$
0.1	0.7	0.5	0.5	7.0	0.175383
0.2					0.174711
0.3					0.174042
	0.8				0.186256
	0.9				0.19701
		0.6			0.176651
		0.7			0.177956
			0.6		0.173908
			0.7		0.172443
				8.0	0.179449
				9.0	0.183584

Table 3.3: Numerical outcomes of $Sh_x Re_x^{-1/2}$ via various parameters with $M = \beta = \lambda_1 = Gr_T = Gr_C = 0.1, Br = \theta_w = 0.5, Pr = 7.0, Rd = 0.7$.

Sc	f_w	γ	$Sh_x Re_x^{1/2}$
0.5	0.5	0.5	0.448373
0.6			0.527177
0.7			0.605981
	0.6		0.495655
	0.7		0.542937
		0.6	0.438522
		0.7	0.429831

3.6 Conclusion

Our motive of the present study is to investigate entropy optimisation of 2D Steady, incompressible, Natural convection MHD flow of electrically conducting fluid over vertical stretching sheet in the presence of first-order velocity slip. The problem is solved using HAM. The major findings of this study are

- Velocity reduces compared to rising M, γ and f_w values.
- Temperature declines with increase in Pr, while enhances with increase in Rd, θ_w and Br.
- For larger Sc and f_w values, concentration decreases.
- N_G augmented when increment occurs in M, L^* and Br.
- Br and L^* have opposite effect on Bejan number.
- Be declines with increase in M when $\eta < 1$, for $\eta > 1$, Be enhanced.
- Skin friction coefficient enhances via γ and Gr_T.
- Nusselt number enhances against rising values of Pr, θ_w and Rd.
- Skin friction coefficient and Sherwood number have opposite behaviour for f_w.